Optical and Electrical Modeling of Nanocrystalline Solar Cells

This chapter focuses on theoretical modeling of nanocrystalline semi-conductor films

A typical dye-sensitized solar cell is composed of

1- a nanocrystalline titanium dioxide (TiO2) film
2- dye-sensitizers,
3- an electrolyte,
4-a transparent conductive substrate,
5-and a counter electrode

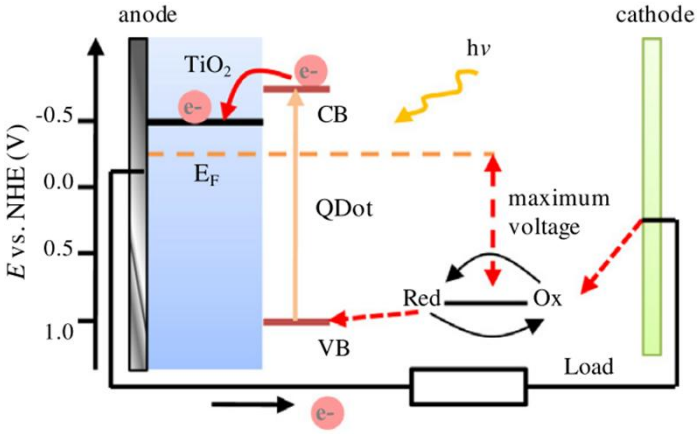

Fig. 14. Scheme of a QDsSSC and its working mechanism.

A photovoltage loss stems from the following two driving forces: the electron injection from a dye-excited state into the TiO2 conduction band, and the dye regeneration by redox species.

a straightforward method of conventional device modeling is applicable, dividing the electrode into spatial finite elements and formulating the Poisson and current equations.

required huge memory and a long computing time.

To avoid ⟹, a mean-field expression, such as a pseudo-homogeneous Approximation in a macroscopic electrical simulation of the dye-sensitized electrode

History of the simulations

1- Södergren et al in 1994

-model for photoelectron transport in a bare TiO2 porous film,
-applied to current–voltage characteristics simulations of a dye-sensitized solar cell.
-Neglecting redox species in the electrolyte, they modeled only electron transport in the semiconductor matrix.
In addition, they treated the nanoporous electrode as an apparent continuum. As a result, an analytical formula was provided

2-Advanced models that consider redox species in the electrolyte were presented by Usami and Ferber et al. by adopting the pseudo-homogeneous approximation to the semiconductor.

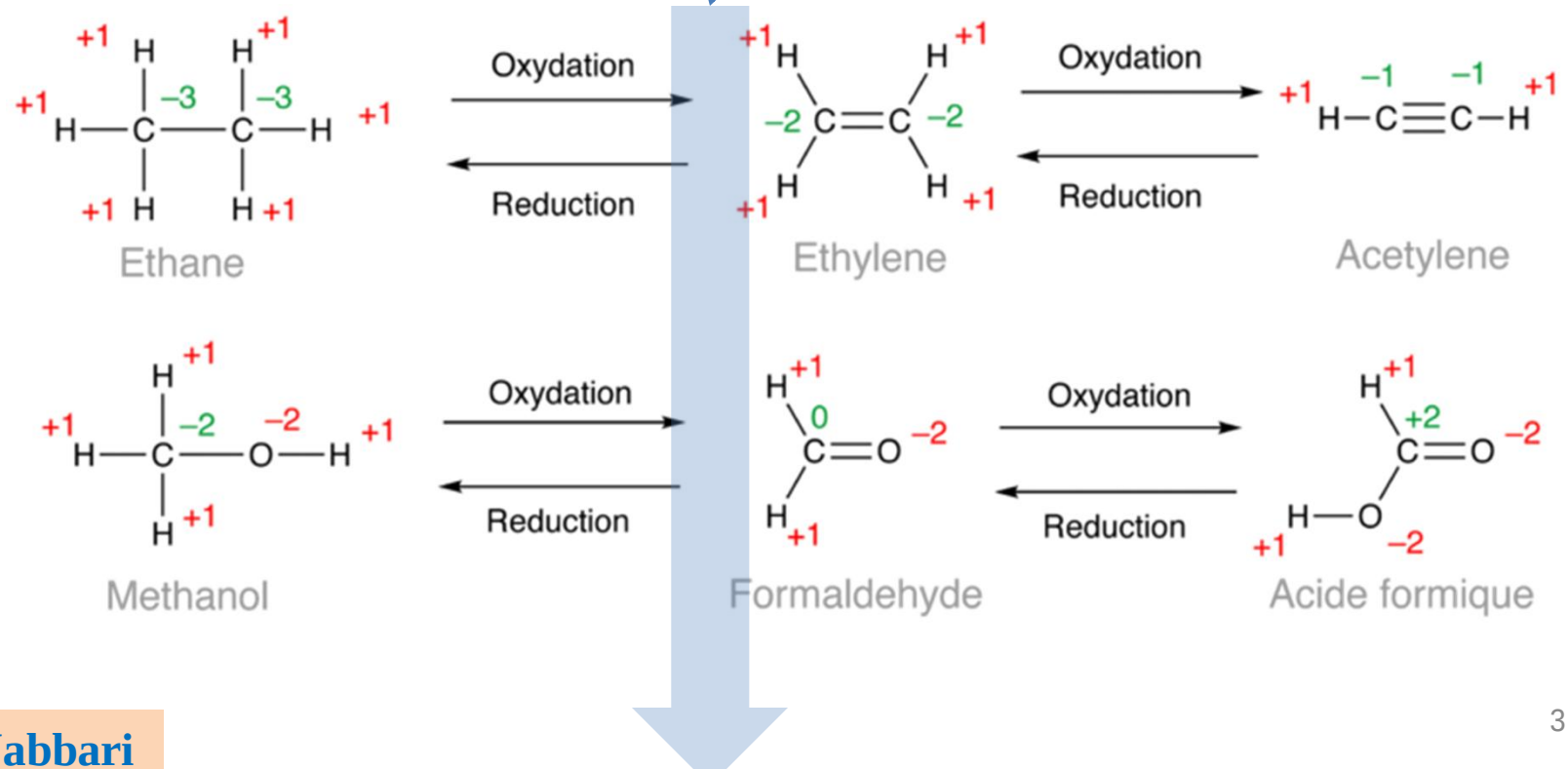

اُکسایـــش و کاهش (به انگلیسی: Redox) نام کلی واکنش‌های شیمیایی است که مایه تغییر عدد اکسایش اتم‌ها می‌شوند. این فرایند می‌تواند دربرگیرنده واکنش‌های ساده‌ای همچون اکسایش کربن و تبدیل آن به کربن دی‌اکسید و کاهش کربن و تبدیل آن به متان و یا واکنش‌های پیچیده‌ای چون اکسایش قند در بدن انسان طی واکنش‌های چند مرحله‌ای باشد.

با کمی اغماض علمی می‌توان این فرایند را انتقال یک یا چند الکترون از یک اتم، مولکول یا یون به یک اتم، ملکول یا یون دیگر دانست.

در هر واکنش اکسایش و کاهش اتم یا مولکولی الکترون از دست می‌دهد (اکسایش) و اتم یا مولکولی دیگر الکترون جذب می‌کند (کاهش) می‌یابد. در چنین واکنشی مولکول دهنده اتم اکسیده شده و ملکول گیرنده کاهیده می‌شود.

در واقع تعریف ابتدایی اکسایش واکنش یک ماده با اکسیژن و ترکیب شدن با آن بوده‌است، اما با کشف الکترون اصطلاح اکسایش دقیق‌تر تعریف شد و کلیه واکنش‌هایی که طی آن ماده‌ای الکترون از دست می‌دهد اکسایش نامیده شدند. اتم‌اکسیژن می‌تواند در چنین واکنشی شرکت داشته یا نداشته باشد.

در اثر اکسایش عدد اکسایش معمولی یک اتم یا اتم‌های یک مولکول در پی حذف الکترون‌ها افزایش می‌یابد. برای نمونه آهن (II) می‌تواند به آهن (III) اکسید شود.

$Fe^{2+} \rightarrow Fe^{3+} + e^-$

However a numerical simulation with a computer is necessary.

Unfortunately, there are some simulations to which this approximation is inapplicable, that is, photoelectron random walk involving trapping/detrapping processes in nanoparticles.

Especially, influences of the particle necking and coordinating number on the electron transport cannot be simulated without going into the geometric details of the porous photoelectrode.

Monte Carlo methods based on the continuous-time random walk (CTRW)

multiple trapping (MT)

These simulations follow traces of electrons walking in an imaginary trap lattice created in a computer program with random numbers

Monte Carlo simulations also have been applied to analyses of electron recombination dynamics, and satisfactory agreement with experimental data

The first simulation of light transmission in the nanocrystalline electrode considered multiple scattering effects, independent scattering was assumed

In this chapter:

- optical modeling of nanocrystalline TiO2 films and application of light scattering
- first, an equivalent circuit;
- second, Monte Carlo simulations of photoelectron transport in nanocrystalline articles;
- third, formulation of differential equations expressing transport of electrons and redox species in the solar cells, and numerical solutions of these equations

Light Scattering Properties of Nanocrystalline TiO_2 Films

For a film consisting of randomly distributing small particles, the simplest scattering model is the independent scattering model.

The scattering rate a for the simplest model has been already presented

$$\alpha = \beta\lambda^{-4}a^3$$

where λ is the wavelength of incident light and a the radius of a particle.

, β depends on the refractive index, fractional volume, and distribution of the particles

β is formulated analytically with the refractive indices of the particles n_s and the nanocrystalline film n, and the fractional particle volume f [24–26],

$$\beta = 2f(2\pi n)^4 \left| \frac{n_s^2 - n^2}{n_s^2 + 2n^2} \right|^2 \qquad (2.2)$$

The light hemispherical (= collimated + diffused) transmittance T is

R is the specular reflectance on the film surface and d the film thickness.

Consequently $\Rightarrow$ $$\ln(T) \propto \frac{\beta(f, n_s, n)}{2} \lambda^{-4} a^3 d$$

$\Downarrow$

However, for dense media, the scattering rate evaluated with this literal independent scattering model is much greater than experimental results.

$\Downarrow$

Annealing in the film preparation makes the particles interconnected, and the charges can transport between the electrodes

For the multiple scattering effects, $\ln(T) \propto \lambda^{\gamma}$ where γ increases from -4

Application of Light Scattering to Dye-Sensitized Solar Cells

Practically, a nanocrystalline film → powder=P25 = 50 nm diameter

In a dye-sensitized solar cell, a nanocrystalline film is the photoactive electrode

Light scattering in the photoactive electrode → light absorption ↑ because: optical length ↑, optical confinement ↑

The optical length depends on the paths of photons in the film.

Without scattering

absorbance is $\alpha_{abs} d$, where α_{abs} and d are the absorption coefficient and the film thickness

If photons are scattered in the film, the photons feel the film thicker than d; because of this increase of the optical length,

And

Optical confinement is also expected; because of a large average refractive index of the TiO2 nanocrystalline film

Although the scattering intensity increases in proportion to the particle diameter for the Rayleigh scattering

The ray-tracing Monte Carlo simulation has been widely applied to analyses of light transmission in a living body in infrared (IR) spectroscopy, such as the optical computer tomography [30].

Since a living body is also a strong light scattering medium, the same method is applicable to analyses of the light scattering in the nanocrystalline electrode.

A scattering medium is characterized by the following parameters:

- the scattering coefficient, α_{sct} [m^{-1}],
- the absorption coefficient, α_{abs} [m^{-1}],
- e angle distribution of the scatter-ing intensity by a scattering center, $p(\theta)$

For simplicity, we assume a homogeneous medium and monochromatic light.

probability that a photon getting into the medium is transmitted without scattering or absorption through a length, l ⇒ $\exp\{-(\alpha_{sct}+\alpha_{abs})l\}$

transmission length, L

$$L=-\frac{1}{\alpha_{sct}+\alpha_{abs}}\ln(Rnd[0,1])$$

$Rnd[0,1]$ is a random number between 0 and 1

if $Rnd[0,1] < \alpha_{sct}/(\alpha_{sct}+\alpha_{abs}) \rightarrow$ scattering,
if $Rnd[0,1] < \alpha_{abs}/(\alpha_{sct}+\alpha_{abs}) \rightarrow$ absorption.

If absorbed, the location is recorded; if scattered, relative scattered direction (θ,φ) is

$$\theta = f^{-1}(Rnd[0,1]) \quad (2.5)$$

$$\varphi = 2\pi Rnd[0,1]$$

$$f(\theta)=\int_0^{\theta} p(\theta)\,d\theta, \quad f(\pi)=1 \quad (2.6)$$

The same procedure is repeated until the photon is absorbed.

سال 93

SIMULATIONS OF PERFORMANCE OF DYE-SENSITIZED NANOCRYSTALLINE SOLAR CELLS

equivalent circuits,

Monte Carlo simulations.

And numerical analyses based on differential equations

equivalent circuits

$$J = J_{sc} - J_0\left[\exp\left(\frac{qV}{n\kappa_B T}\right) - 1\right]$$

$$J = J_{sc}\left[1 - \exp\left(\frac{q(V - V_{oc})}{n\kappa_B T}\right)\right]$$

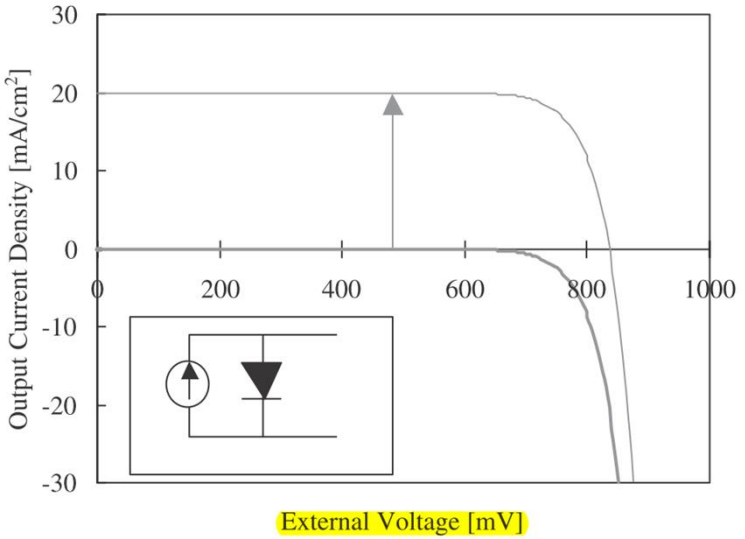

Equation (3.2) is also applicable to dye-sensitized solar cells.

$$J = J_{sc}\left[1 - \exp\left(\frac{q(V - V_{oc})}{n\kappa_B T}\right)\right]$$

is based on the Butler–Volmer equation because the recombination takes place at the semiconductor/electrolyte interface

Ideality factors in dye-sensitized solar cells= 2.0

van de Lagemaat et al explained an ideality factor of 1.0 by a barrier at the TCO/TiO2 interface

and an ideality factor of 2.0 by the electron transfer across the TiO2/electrolyte interface,

Rau et al. [42] expressed the equivalent circuit as a series connection of two diodes.

However, for dye-sensitized solar cells, under illumination, the current–voltage characteristics cannot be calculated from the photocurrent source and the dark diode property.

A disadvantage of the equivalent circuit is that the relation between the model and the energy conversion processes is unclear.
Recent progress of fundamental studies on the ideality factor described above makes this disadvantage less important.

Monte Carlo Simulation

For dye-sensitized solar cells, a trace of a photoelectron in a nanoparticle or a nanocrystalline film has been simulated with random numbers.
With the Monte Carlo simulation, dynamics of the electron diffusion and recombination has been studied;
static properties, such as the current–voltage characteristics, are not usually fit for the Monte Carlo simulation.

In trap-dotting materials, electron transport has been explained by the following two models: continuous-time random walk (CTRW) or the multiple trapping (MT).
While MT explicitly considers a difference between electrons transported in the conduction band and electrons localized in the trap levels,
the difference is unclear in CTRW.

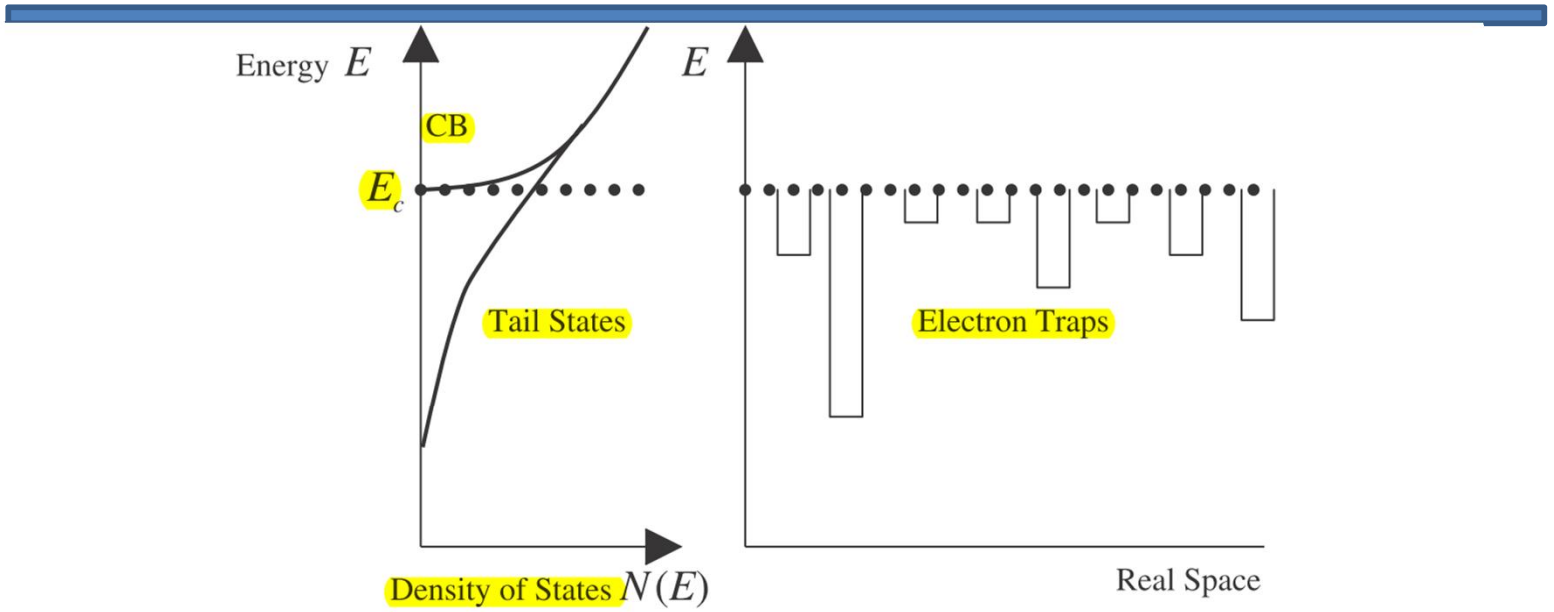

Fig. 2. Electronic states of TiO_2 nanoparticles. CB represents the conduction band. The tail states consist of the localized trap levels in the real space, and "hopping" between the localized trap levels is the predominant electron transport process.

The tail states have the following energy distribution:

$$N(E) = \frac{N_{tot}}{m_c} \exp\left(\frac{E - E_c}{m_c}\right)$$

$N(E)$ is the density of states at the energy

N_{tot} the total trap density,

$m_c = 60 - 100\,\text{meV}$ is reported experimentally for TiO_2 nanocrystals

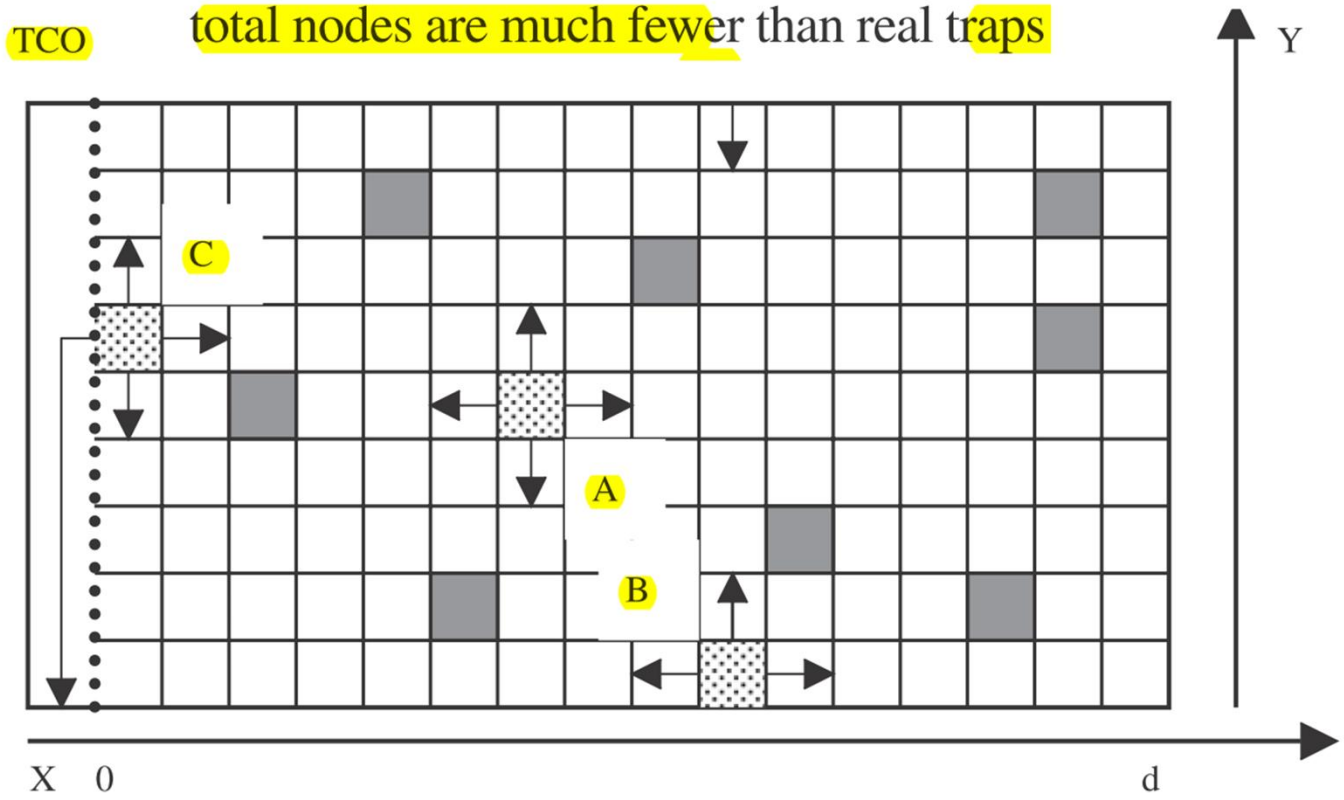

Fig. 3. An outline of the Monte Carlo simulation. Adopting the pseudo-homogeneous model, the nanocrystalline electrode is treated as a cubic lattice. Each node represents an electron trap. Shadows express electron-occupied traps. An electron in a trap can move to the neighboring traps if the destination is unoccupied (A). At the edges, the periodic boundary conditions are assumed (B). When an electron reaches the TCO, the electron becomes the external current (C).

$$E_T - E_c = m_c \ln(Rnd[0,1])$$

$$f(E_T) = \frac{1}{1+\exp(E_T - E_F/\kappa_B T)}$$

$Rnd[0,1] < f(E_T)$: the trap is occupied,

$Rnd[0,1] > f(E_T)$: the trap is empty.

the waiting time, τ_r,

$$\tau_r = \frac{\exp(E_T - E_c/\kappa_B T)}{\nu_{th}}$$

where ν_{th} is a frequency around $10^{12} - 10^{13}\ s^{-1}$

Numerical Analysis Based on Differential Equations

In conventional solar cells based on a solid p–n junction, solar cell performance has been analyzed with computer simulation programs, such as "PC-1D"

However, photogenerated charge carriers in a dye-sensitized solar cell have a different spatial distribution from those in the conventional solar cells.

PC-1D cannot be employed for dye-sensitized solar cells in which the carrier transport occurs by the diffusion, rather than the drift by a built-in potential,
because of a negligible macroscopic electric field across the bulk of the photoanode owing to screening by the high-ionic-strength electrolyte

On the basis of a theory in batteries [47],
the porous photoelectrode is treated as a superposition of two continua

one represents a pore-filling solution

solid semiconductor matrix

Current density i1 and i2 are introduced for electrons in the matrix and ions in the solution

سال 93

The macroscopic current density in the electrode is obtained as *the sum of i1 and i2*.

The equations for the dye-sensitized solar cell are represented in one-dimensional form:

$$\frac{di_1}{dx} + \frac{di_2}{dx} = 0 \qquad (3.7)$$

$$i_1 = \varepsilon \mu_n n \frac{d\varepsilon_F}{dx} \qquad (3.8)$$

$$i_2 = \frac{2\varepsilon(\mu_3 - 3\mu_1)}{2 + \ln\gamma} C_3 \frac{d\mu}{dx} \qquad (3.9)$$

$$\frac{di_1}{dx} = -e\Phi\alpha \exp(-\alpha x) + ef_{rec} \qquad (3.10)$$

quasi-Fermi level in the semiconductor matrix

electron density in the semiconductor matrix,

the triiodide ion concentration in the solution,

γ is the activity coefficient of the ions

Here, the redox couple in the solution is I^-/I_3^-.

and μ without a subscript ⟹ chemical potential of the ions,

μ with a subscript is the mobility; the subscripts of n, 1, and 3 in the mobility represent electron, iodide ion, and triiodide ion, respectively.

ε a correction factor

α the light absorption coefficient of dye-sensitizers, and Φ the light intensity. For simplicity, the incident light is assumed to be monochromatic.

The first equation represents the charge conservation. The second and third equations are the current equations for electrons and ions, respectively. In these equations, both the diffusion and drift terms are implicit. However, only the diffusion is taken into account because the macroscopic electric field across the electrode is negligible owing to screening by the high-ionic-strength electrolyte. The correction factor ε represents decrease of the mobility due to the nanocrystallization. In Eq. (3.9), from the net chemical reaction in the electrolyte: $I_3^- + 2e^- \leftrightarrow 3I^-$, the following is assumed: $dC_1:(-dC_3) = 3:1$, denoting the iodide ion concentration by C_1. The last equation represents the charge separation; here, the light absorption and the recombination are described. In the light absorption term, which is the first term on the right-hand side, the solar cell is illuminated from the interface between the nanocrystalline electrode and the TCO electrode ($x = 0$). The recombination term is represented as f_{rec}.

By: Dr. Jabbari

$$f_{rec} = f_{rec,low} + f_{rec,high} = \frac{n^{\beta_{low}} C_3}{\tau} + \alpha\Phi\left(\frac{n}{n_{r,d}}\right)^2 \exp(-\alpha x)$$

are for a low light intensity and a high light intensity,

Since the diffusion length is the square of the product of the diffusion coefficient and the lifetime,

this is partly compensated by an increase of the electron lifetime with lowering the light intensity making the incident photon-to-current conversion efficiency (IPCE) less dependent on the light intensity

see Fig. 4 and Table 1

Table 1
Parameters of the theoretical model

Symbols	Employed values	Notes
λ	650 nm	Wavelength of incident light
$\alpha(\lambda)$	$1.95 \times 10^{5}\,m^{-1}$	Absorption coefficient of electrode
D_s	$5.0 \times 10^{-5}\,cm^2\,s^{-1}$	Diffusion coefficient of electrons in semiconductor matrix
$D_{I^-}, D_{I_3^-}$	$2.6 \times 10^{-6}\,cm^2\,s^{-1}$	Diffusion coefficients of iodide and triiodide in electrolyte pores
d	10 μm	Nanocrystalline electrode thickness
n_i	$3.1 \times 10^{21}\,cm^{-3}$	Effective density of states of conduction band

Notes: 100% light reflectance at the Pt-counter-electrode mirror is also assumed; concentrations of triiodide in the dark are 50 ± 1 mM.

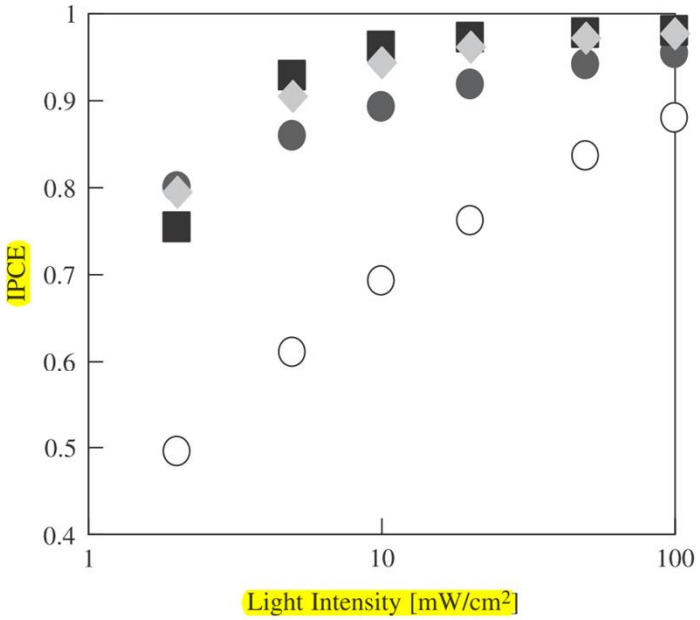

Fig. 4. Dependence of IPCE on low light intensity. Solid circles: $\beta_{low} = 0.5$, $\tau = 4.0 \times 10^{12}\,m^{-1.5}\,s$; solid diamonds: $\beta_{low} = 0$, $\tau = 25\,s$; solid squares: $\beta_{low} = -0.5$, $\tau = 1.5 \times 10^{-10}\,m^{1.5}\,s$; open circles: $\beta_{low} = 0.5$, $\tau = 1.0 \times 10^{12}\,m^{-1.5}\,s$. The values of the parameters in Table 1 are employed. We calculate dependence of IPCEs on light intensities, 2–100 $mWcm^{-2}$, with the presented model. In low intensities, the recombination term $f_{rec,high}$ becomes very small because $n_{r,d}$ is expected to be greater than $10^{17}\,cm^{-3}$. Although this term may be nonnegligible at relatively high light intensities, we disregard $f_{rec,high}$ to emphasize influences of the term $f_{rec,low}$ here. In Eq. (3.11), a definite value of τ is not known for real dye-sensitized solar cells. Thus, in the solid notations, diffuse lengths of electrons in the electrodes are assumed to be roughly 7–10 μm at 1 $mWcm^{-2}$. For comparison, the results of a fourth in τ at $\beta_{low} = 0.5$ are also shown as the open circles. The results indicate that the IPCE decreases with decreasing the incident light intensity; this reproduces experimental decrease of IPCE with decreasing illumination intensity [57].

By: Dr. Jabbari

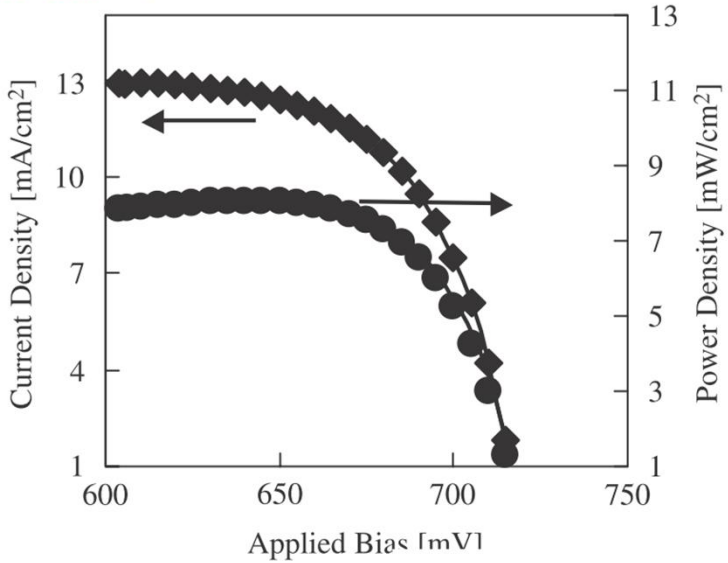

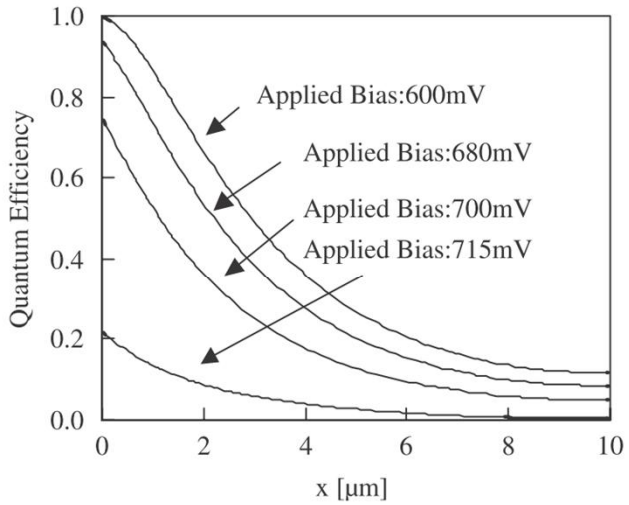

Fig. 5. Current–voltage characteristics and dependence of quantum efficiency on applied bias V for $n_{r,d} = 4 \times 10^{17}\,\mathrm{cm}^{-3}$. The values of the parameters in Table 1 are employed. The other parameters were $\Phi = 50\,\mathrm{mWcm}^{-2}$, $\beta_{low} = 0.5$, and $\tau = 4.0 \times 10^{12}\,\mathrm{m}^{-1.5}\,\mathrm{s}$. x is the distance from the TCO/TiO_2 interface.

Chapter 4

Mathematical Modelling of the Refractive Index and Reflectivity of the Quantum Well Solar Cell

The first quantum well solar cell showed remarkable promise. A standard AlGaAs/GaAs p–i–n solar cell was approximately 9% efficient at the time. The introduction of the quantum wells produced an efficiency of 14%

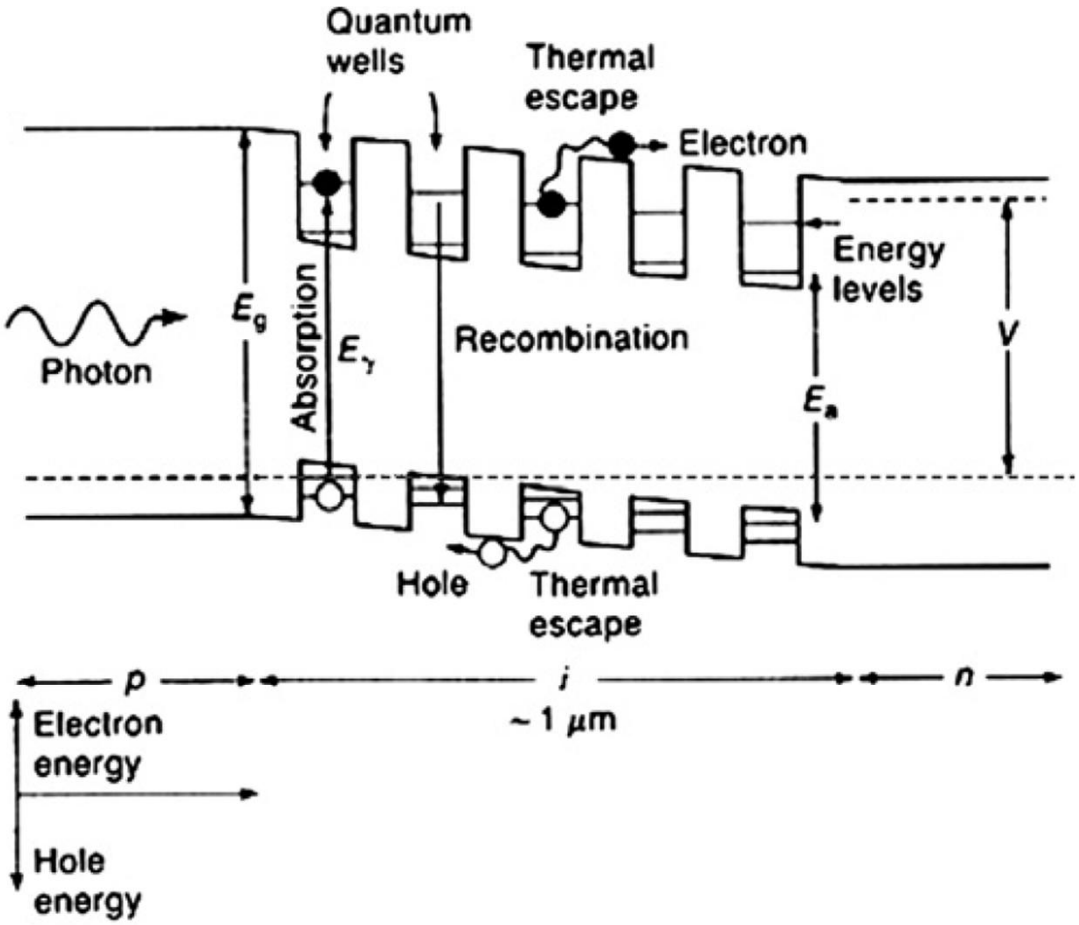

Fig. 1. Schematic of a quantum well solar cell.

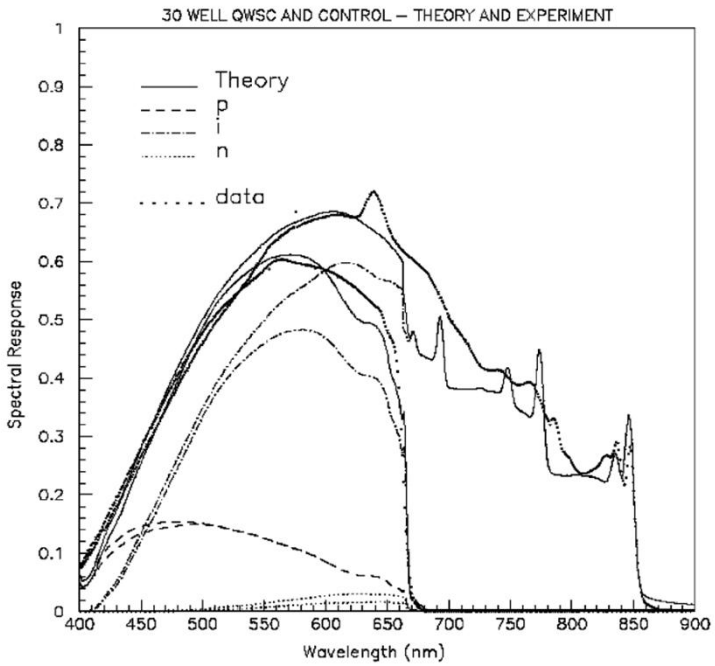

Fig. 2. Spectral response (heavy dots) for a 30-well AlGaAs/GaAs QWSC and a homostructure AlGaAs control cell. The i-region has the same thickness in both cases. Thin lines are fits with the programme SOL. The p-, i- and n-region contributions are shown separately.

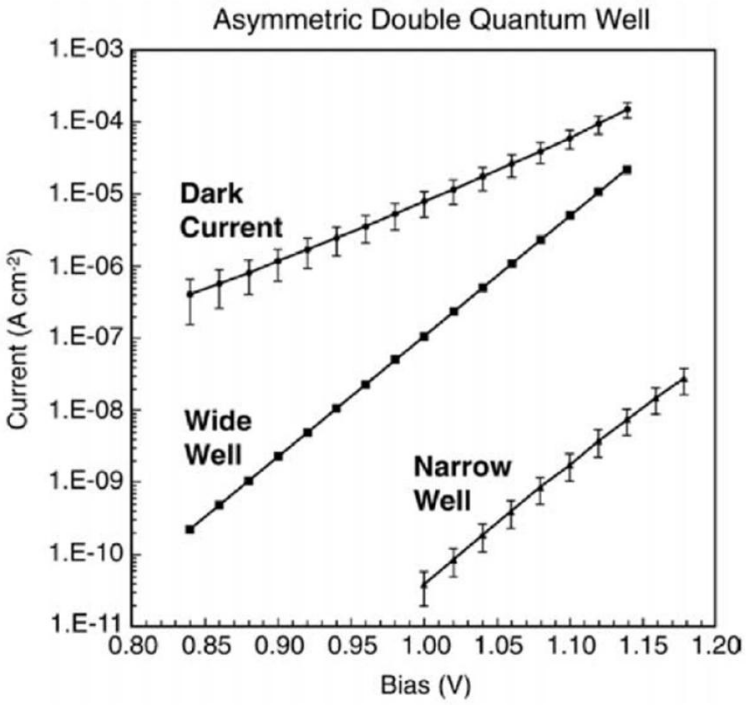

Fig. 3. Radiative currents extracted from the wide and narrow wells of DQW devices compared with the dark currents of the devices.

double (DQW) quantum well

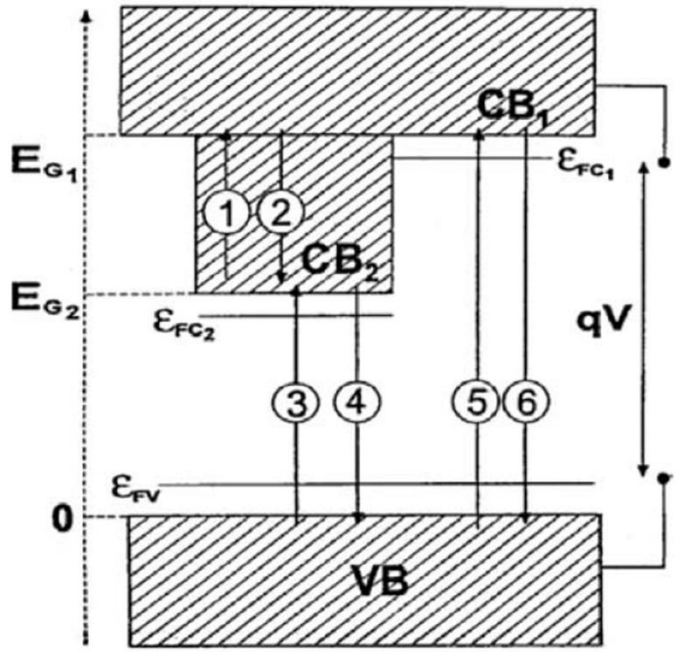

Fig. 5. Schematic representation of the radiative transitions in the model of Ref. [14].

The effects of cell dimensions such as QW and intrinsic region length on overall structure efficiency have been explored previously for InP-based QWSC [10, 11]. The paper consisted of "strained" structures grown with varying QW and intrinsic region lengths, experimentally evaluated under a solar spectrum. The findings showed lengths of 5 and 500 nm, respectively generating greatest efficiency (approximately 26%).

In more recent times research conducted by Bremner [21] investigated the detailed balance efficiency limits through non-uniform quasi-Fermi levels. The approach taken here allows for the possibility of photons with energies below the QW energy gap to be absorbed by photocarriers in the quantum wells, thus providing the energy required to escape the QW confinement. Further features of the approach includes effects of reduced carrier captured in the quantum wells due to hot carrier transport, this directly relates to the reduction in radiative recombination and hence increases the limiting efficiency to approximately 63%.

In this chapter, the author intends to present new models relating to the refractive index and reflectivity of quantum well solar cells.

2. MODELLING THE QWSC'S REFRACTIVE INDEX AND REFLECTIVITY WITH THE MODIFIED SINGLE EFFECTIVE OSCILLATOR MODEL

The determination of the refractive index → the Kramer–Kronig relationship.
↓
the complex dielectric constant

This complex relationship can be approximated using the Modified Single Effective Oscillator (MSEO) model. Associated with the refractive index of the cell is the reflectivity or reflective loss.

2.1. Refractive Index Modelling

Kramers–Kronig relationship for the complex dielectric

$$\varepsilon(\omega) = \varepsilon_1(\omega) + i\varepsilon_2(\omega) \qquad (1)$$

where
$n = \sqrt{\varepsilon_1(\omega)}$ is the refractive index
$\varepsilon_2(\omega)$ is associated with the absorption coefficient.
This complex equation may be replicated through the MSEO model.

$$\varepsilon_1 - 1 = \frac{2}{\pi} P \int_0^{\infty} \frac{E' \varepsilon_2(E') \mathrm{d}E'}{E'^2 - E^2}$$

where P denotes the principal value of the integral.

Considering $\varepsilon_1(E)$ for the direct energy gap (E_Γ) and values below equalling zero, one can expand Eq. (2) to be

$$\varepsilon_1(E) - 1 = \chi(E) = \frac{2}{\pi} \int_{E_\Gamma}^{\infty} \varepsilon_2(E') \left[\frac{1}{E'} + \frac{E^2}{E'^3} + \frac{E^4}{E'^5} + \cdots \right] \mathrm{d}E' \qquad (3)$$

For $E < E_\Gamma \leq E'$

$$\chi(E) = M_{-1} + M_{-3} E^2 + M_{-5} E^4 + \cdots$$

where

$$M_i = \frac{2}{\pi} \int_{E_\Gamma}^{\infty} \varepsilon_2(E) E^{\mathrm{i}} \, \mathrm{d}E$$

$$\varepsilon_2(E) = \eta E^4$$

For $E_\Gamma \leq E \leq E_f$

Otherwise, equal to zero for other energies.

Integrating Eq. (5) gives

$$M_{-1} = \frac{\eta}{2\pi}(E_f^4 - E_\Gamma^4)$$

$$M_{-3} = \frac{\eta}{\pi}(E_f^2 - E_\Gamma^2)$$

$$E_f = (2E_o^2 - E_\Gamma^2)^{1/2}$$

$$\eta = \pi E_d / 2E_o^3 (E_o^2 - E_\Gamma^2)$$

Expanding Eq. (4) and substituting into (7) we obtain the complete refractive index given as [27]

$$n^2 = 1 + \frac{E_d}{E_o} + \frac{E_d}{E_o^3}E^2 + \frac{\eta}{\pi}E^4 \ln\left(\frac{2E_o^2 - E_g^2 - E^2}{E_\Gamma^2 - E^2}\right) \quad (8)$$

where
$E = \hbar\omega$ is the photon energy (eV) and
$\hbar$ the Planck's constant divided by 2π

$$\omega = \frac{2\pi c}{\lambda}$$

c is the speed of light and
λ the wavelength of light.

The determination of the remaining parameters has been obtained through experiment

For the oscillator energy

$$E_o = A + BE_\Gamma$$

where
E_Γ is the lowest direct band gap.

$$A \approx 2.6$$
$$B \approx 0.75 \qquad (9)$$

For the dispersion energy

$$E_d = \frac{F}{E_o} \qquad (10)$$

where
F is related to the Kramer–Kronig relationship.

$$\varepsilon_1(\omega) - 1 = \omega_p^2 \sum_n \frac{f_n}{(\omega_n^2 - \omega^2)} \qquad (11)$$

where

$$F = \omega_p^2 f_n$$

where

$$\omega_p^2 = \frac{4\pi q^2}{m_h}\frac{N}{\Omega} \text{ is the plasma frequency} \qquad (12)$$

N/Ω is the number of valence electrons per unit volume.
q and m_h are the electron charge and effective mass of the valence band particle (hole), respectively.
f_n is the oscillator strength and ω_n the frequency of the corresponding transition.

$$f_n = \frac{2\hbar}{m^* \omega}\left|\left\langle \Psi_i \left| \frac{\partial \Psi_f}{\partial x} \right\rangle\right|^2 \qquad (15)$$

where
$m^* = m_e m_h/(m_e + m_h)$ is the effective mass of the particles
ω the transition frequency
Ψ_i and Ψ_f the wave functions of the respective energy levels associated with the transition.

For simplicity, the author has assumed the potential of the quantum wells to be significantly large so that they can be classified to be infinite wells. The barrier lengths are also assumed to be significantly large that "tunnelling effects" between the wells are not possible. Assuming the electric field (F below) to be perpendicular to the quantum well layers and the device to be quasi one-dimensional (x). This yields the boundary conditions of the wave functions within the well as

$$\Psi(x = 0) = 0$$

$$\Psi(x = L) = 0$$

It can be shown that the Schrödinger wave equation for such a configuration is given as [30]

$$\left(-\frac{\hbar^2}{2m}\frac{\partial^2}{\partial x^2} + |q|Fx - E_n\right)\Psi_{i/f} = 0$$

2.2. Approximating Quantum Wells

Determination of the refractive index of multiple quantum well

The simple concept is the replacement of the multiple quantum well layers with a single homogenous layer yielding an average refractive index

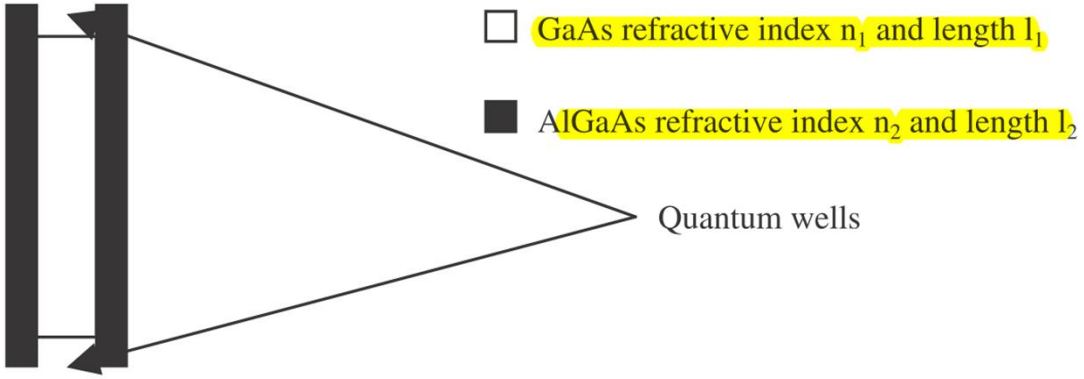

Fig. 2. Repeating layers.

Following the Alman analysis

$$n^2 = \frac{\sum_j n_j^2 d_d}{\sum_j d_j} = \frac{n_1^2 l_1 + n_2^2 l_2}{l_1 + l_2}$$

for transverse electric (TE).

$$\frac{1}{n^2} = \frac{\sum_j \frac{1}{n_j^2} d_d}{\sum_j d_j} = \frac{\frac{l_1}{n_1^2} + \frac{l_2}{n_2^2}}{l_1 + l_2}$$

for transverse magnetic (TM).

By: Dr. Jabbari

2.3. Electric Field Effects on the Refractive Index of Multiple Quantum Wells

In this section the new approach documented above will be utilised to investigate the effects of electric field on the refractive index of the multiple quantum well solar cell.

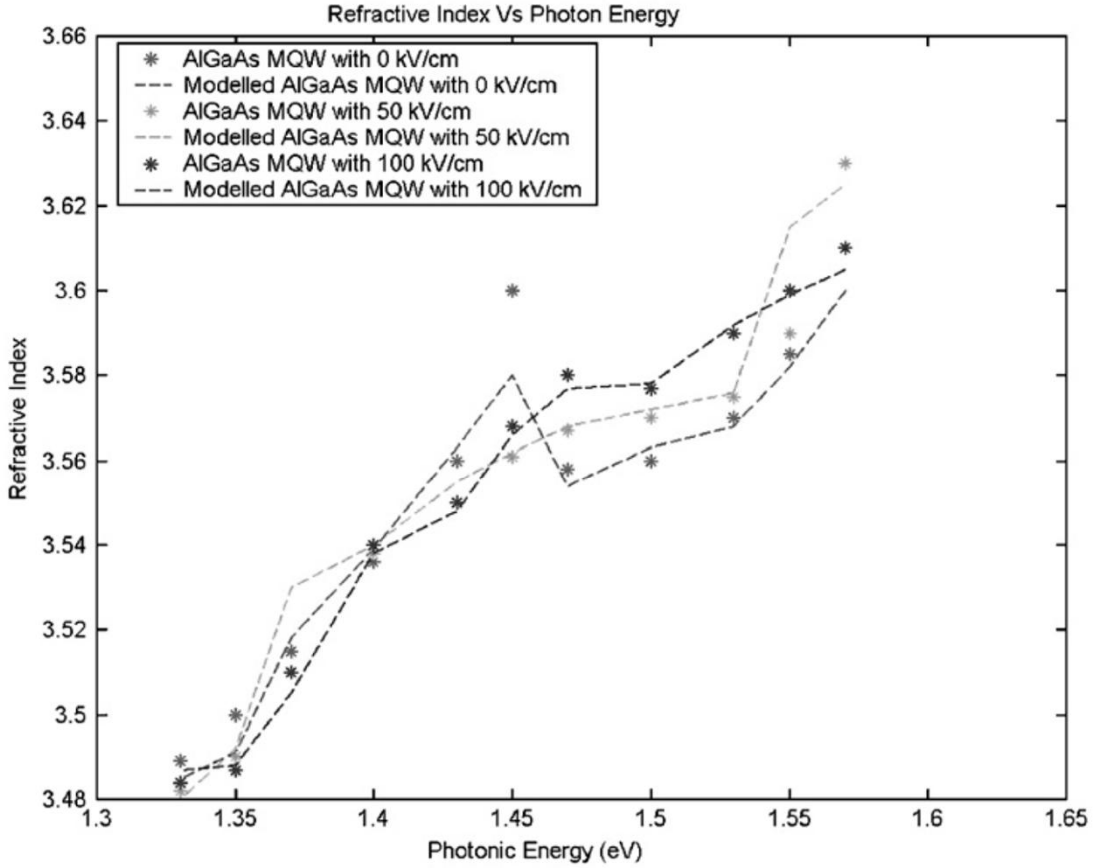

Fig. 3. Refractive index of quantum wells within a QW modulator. A comparison between model and theoretical data with an electric field of 0–100 kV/cm is considered.

Table 1
Refractive index versus photonic energy for a given electric field

Variable	Refractive index								
Photonic energy (eV)	1.35			1.45			1.55		
Electric field (kV/cm)	0	50	100	0	50	100	0	50	100
Existing model	3.500	3.490	3.478	3.580	3.560	3.580	3.585	3.60	3.600
New model	3.491	3.492	3.488	3.600	3.562	3.566	3.580	3.615	3.610
Inaccuracy (%)	0.20	0.05	0.3	0.50	0.05	0.4	0.1	0.04	0.2

2.4. The Reflectivity of Quantum Well Solar Cells

the Fresnel formula

$$R = \frac{r_1^2 + r_2^2 + 2r_1 r_2 \cos 2\Theta}{1 + r_1^2 r_2^2 + 2r_1 r_2 \cos 2\Theta}$$

with

$$r_1 = \frac{n_0 - n_1}{n_0 + n_1}$$

$$r_2 = \frac{n_1 - n_2}{n_1 + n_2}$$

$$\theta = \frac{2\pi n_1 d_1}{\lambda}$$

n_0 is the refractive index of the incident medium (air) = 1.00; n_1 the refractive index of the anti-reflection coating, and
n_2 the refractive index of the substrate; in this case the QWSC.

The refractive index of the QWSC was achieved through the work covered in Sections 2.1–2.2. These formulae allow the design parameters discussed above in Section 2.3 to be considered. d_1 the thickness of the anti-reflection layer (= 0.00 for no coating).

By: Dr. Jabbari

Table 2
Design parameters for QWSC

Region	ARC	*P*	Intrinsic	*N*
Design 1				
Material	SiN ($n = 2.1$)	AlGaAs/GaAs	AlGaAs/GaAs	AlGaAs/GaAs
		Doping Molar	Doping Molar	Doping Molar
Concentration levels		1.34×10^{18} 0.40	I 0.00	6.0×10^{17} 0.20
Length (nm)	70	150	QW = 50 × 8.7	600

Note: Barrier length = 6.0 nm. A metallic back mirror with 95% reflectivity was not considered in this design.

Table 3
Design parameters for QWSC

Region	ARC	*P*	Intrinsic	*N*
Designs 3–7				
Material	SiN ($n = 2.1$)	AlGaAs/GaAs	AlGaAs/GaAs	AlGaAs/GaAs
		Doping Molar	Doping Molar	Doping Molar
Concentration levels		2.0×10^{16} 0.33	I 0.33	2.0×10^{16} 0.33
Length (nm)	70	140	QW = 5.5	140

Note: Barrier length = 17.0 nm. The number of quantum wells in each structure is 0 (Design 3), 5 (Design 4), 20 (Design 5), 50 (Design 6) and 100 (Design 7).

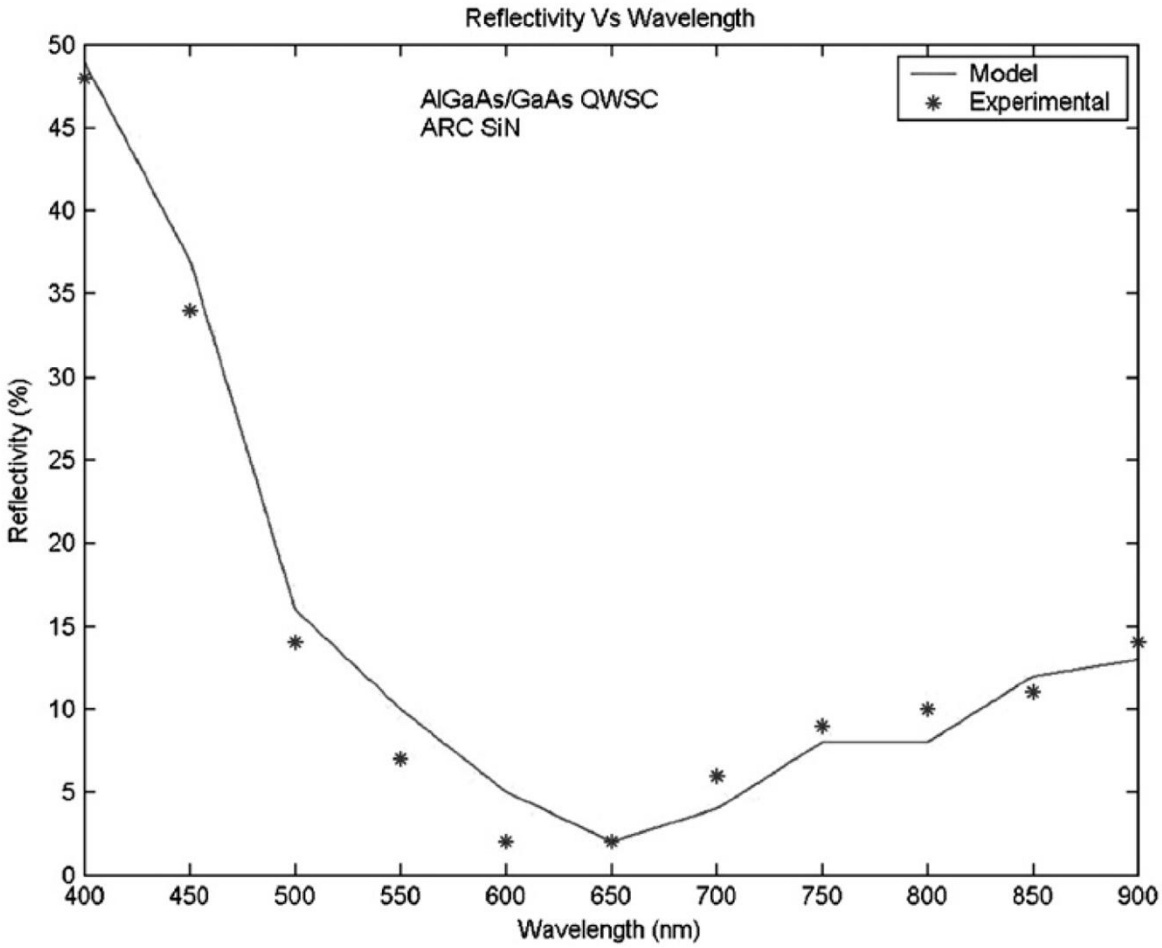

Fig. 4. Theoretical and experimental reflectivity of QWSC structure.

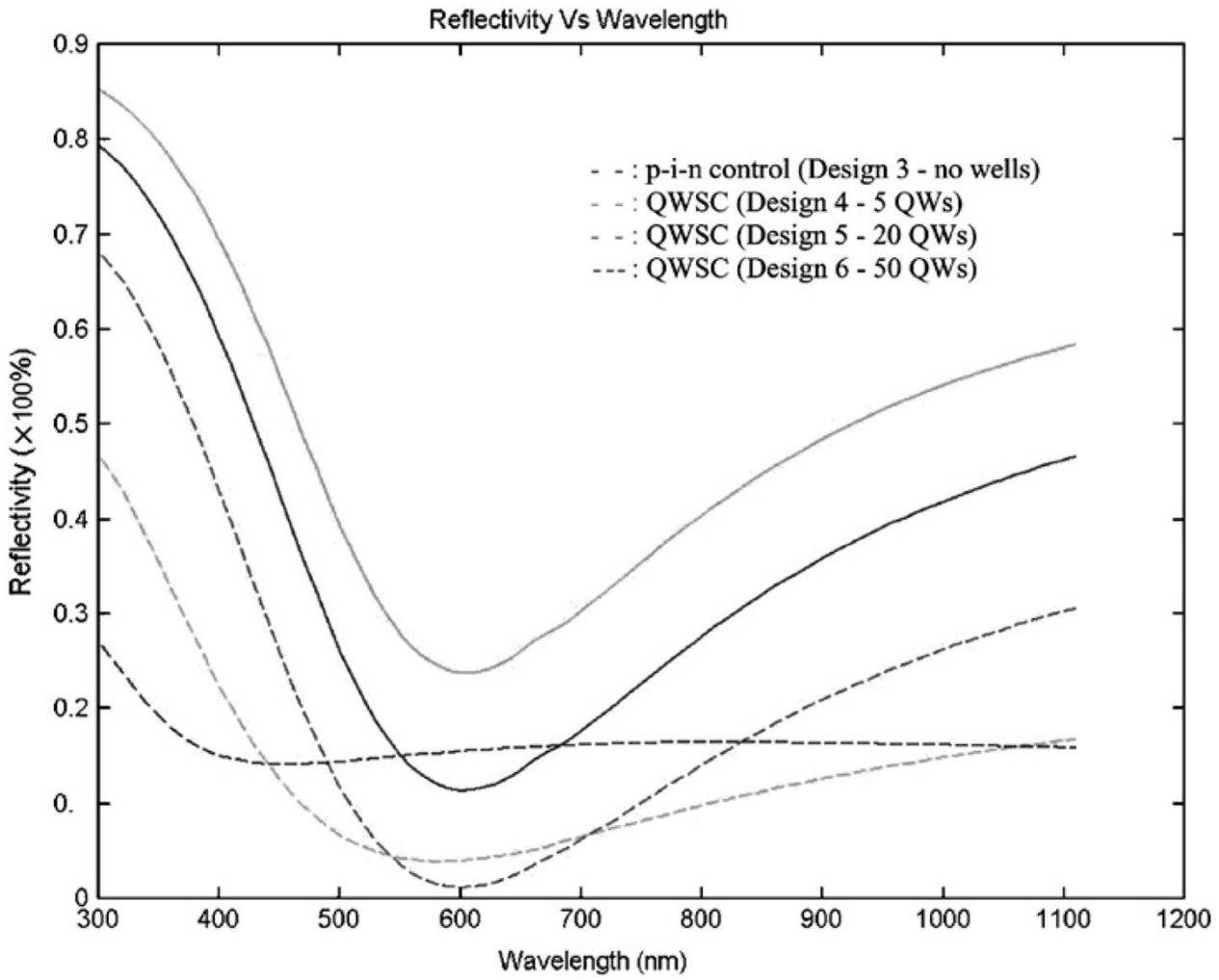

Fig. 5. Reflectivity of QWSC structures with varying quantity of quantum wells within the intrinsic region.

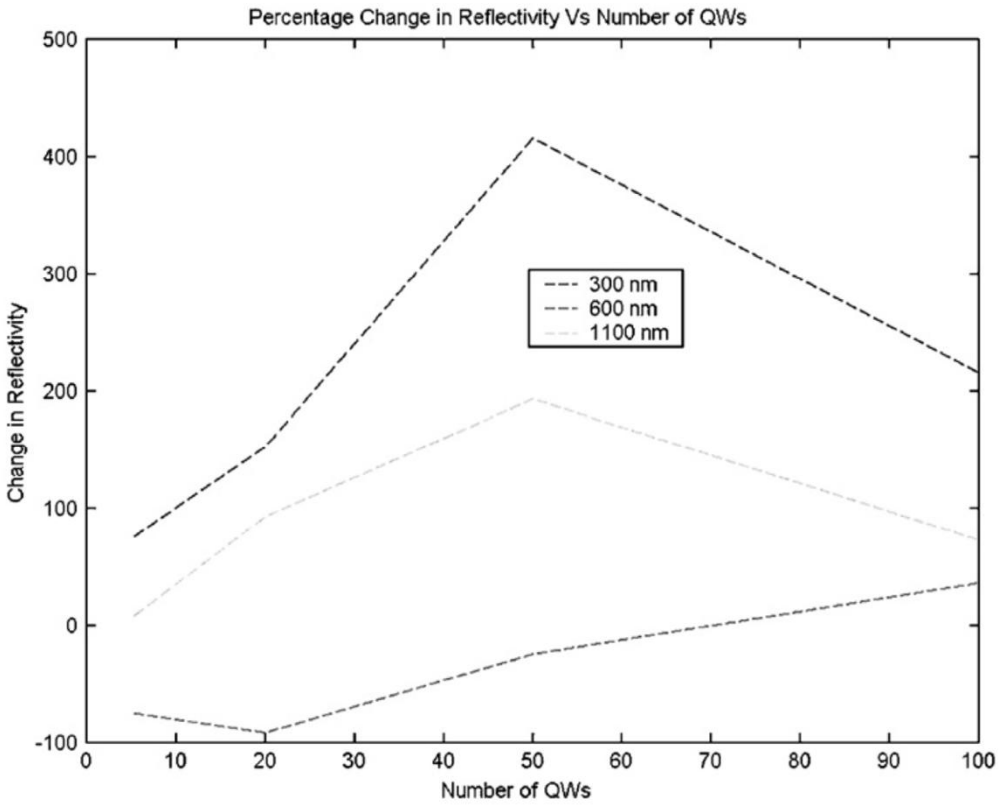

Fig. 6. Percentage change in reflectivity with varying quantity of quantum wells within the intrinsic region.

Table 4
Percentage change in reflectivity induced by the variation in quantum well number

Wavelength (nm)	Design 4 (5 QWs)	Design 5 (20 QWs)	Design 6 (50 QWs)	Design 7 (100 QWs)
300	73.39	152.44	415.45	215.61
600	−74.81	−92.07	−24.87	35.86
1100	5.54	92.37	193.38	72.81